Advances in Simulating Non-congruent phase transitions of Hyperstoichiometric Uranium Dioxide Fuel

M. J. Welland, PhD Candidate
W.T. Thompson and B.J. Lewis, Supervisors
Department of Chemistry and Chemical Engineering,
Royal Military College of Canada, Kingston, Ontario K7K 7B4

Abstract

A model is being developed to simulate UO_2 at very high temperatures incorporating the effects of non-congruent phase transitions. In particular, the melting transformation and the possible 'Λ-transition' is being investigated to help support the design and analysis of experimental work being conducted as part of nuclear safety research. This work includes the interpretation of the behaviour of operating CANDU fuel under upset conditions, where centerline melting may potentially occur (particularly if the fuel is oxidized). The model presented here numerically solves a system of coupled nonlinear differential equations as derived from fundamental principles. The results of the model present here compare well against laser flash experiments in recently published literature.

1. Impetus

Under upset or very high power conditions, particularly with sheath failure, it is possible that the centerline of a fuel pellet will exceed the local melting temperature and begin to melt. Since defective fuel rods allow the coolant to come into contact with the fuel, concurrent oxidization by reaction with H_2O or D_2O is also an important consideration [1].

While approaching the melting temperature, 3120 K, UO_2 may undergo an additional phase transformation located at approximately 2670 K. The exact nature of this transition is currently ill resolved due to extreme conditions required to observe it, but it is currently thought to be a second order, Λ-transition. Its presence is unusually inferred by analysis of cooling curves which may exhibit temperature plateaus due to latent heat effects [2].

Experiments in this region are typically laser-flash type in which heat enters the system through a surface. This is not the case in an operating fuel rod which is heated by fission occurring throughout its volume.

Due to the extreme conditions required to reach these phenomena, experimental data are scarce. It is therefore desirable to have a robust mechanistic model, derived from first principles, capable of simulating these conditions. The introduction of phase transformations adds complexity to fuel behaviour models due to sharply changing material properties and applicable physical phenomena. Models of this type typically require the solution of a set of coupled differential equations in either transient or steady state modes.

2. Phase field modelling

The phase field model adds a scalar variable φ to the problem domain and an associated partial differential equation [PDE] to govern it [3]. This variable is an abstract parameterization of the extent to which a region of material may be considered solid or liquid. It can be interpreted as the local fractional volume that is liquid, or proportional to the regularity of atomic spacing [4]. It is not a conserved quantity. In this development, φ represents the phase change between solid and liquid for clarity, but it can actually represent any phase transformation such as the Λ-transition.

In this analysis, the value of φ varies continuously in the range [0,1] representing solid and liquid respectively. For $\varphi \neq 0,1$ a two phase region is present in which the material is a mix of solid and liquid forming a 'diffuse' interface in contrast to the sharp interface used in other models [5]. This formulation is a very general model which can be shown to reduce to the Stefan condition in the sharp interface limit.

The Theory of Irreversible Processes [TIP] is employed to derive the equations governing φ and its relation to classical heat flux. This theory is founded on the laws of thermodynamics [6] particularly the second law: that in an isolated process, the local entropy produced is positive [7]. As derived in Appendix A, the phase field model requires the solution of the following set of partial differential equations for the temperature T in the generalized heat conduction equation and the phase change φ, respectively:

$$\rho Cp \frac{\partial T}{\partial t} = \vec{\nabla} \cdot k \vec{\nabla} T - \left[p'(\varphi) \Delta H_{Fusion}(T) + K_u'(\varphi)\right] \cdot \frac{\partial \varphi}{\partial t} \tag{2.1}$$

$$\frac{\partial \varphi}{\partial t} = -M_{\phi} \left(\frac{1}{T} \left[p'(\varphi) \cdot \Delta G_{Fusion}(T) - K_u'(\varphi)\right] - \varepsilon_{\varphi}^2 \vec{\nabla}^2 \varphi - \dot{\varphi}_n \right) \tag{2.2}$$

Here the $'$ superscript denotes differentiation with respect to φ and ΔH_{fusion} and ΔG_{fusion} is the enthalpy and Gibbs energy of fusion as obtained from thermodynamic databases such as CALPHAD or FACT. The density ρ, heat capacity *Cp* and thermal conductivity *k* are functions of φ and possibly T. They are assumed to be expressible according to a linear progression between solid and liquid values as shown below for ρ using subscripts S and L to denote the solid and liquid states, respectively:

$$\rho(T,\varphi) = (1 - p(\varphi)) \cdot \rho_S(T) + p(\varphi) \cdot \rho_L(T) \tag{2.3}$$

The function $p(\varphi)$ smoothes φ and allows the enforcement of certain requirements as outlined in the appendix. The function $K_u(\varphi)$ describes the excess surface energy of the material on the boundary between solid and liquid where $\varphi \neq 0,1$. As in other work, these parameters are taken to be [8]:

$$p(\varphi) = \varphi^3 [6\varphi^2 - 15\varphi + 10] \tag{2.4}$$

$$K_u(\varphi) = W \varphi^2 [1 - \varphi]^2 \tag{2.5}$$

Additional phase field constants are given by:

$$W = 6\sigma / \delta \tag{2.6}$$

$$\varepsilon_{\varphi}{}^2 = 12 \sigma \delta / T_m \tag{2.7}$$

$$M_{\varphi} = \frac{k}{5} \left(\frac{T_m}{\delta H_{fus}} \right)^2 \tag{2.8}$$

where σ is the surface energy and δ is a user-chosen measure of the interface thickness and T_m is the melting temperature.

The variable $\dot{\varphi}_n$ describes nucleation of one phase inside another and is given by:

$$\dot{\varphi}_n = \exp\left(-\frac{\Delta G_n^o}{k_B T}\right)\cdot\begin{cases} I_S^o(1-\varphi) & if\ \Delta G_{fus} < 0 \\ -I_L^o\varphi & if\ \Delta G_{fus} > 0 \end{cases} \tag{2.9}$$

where ΔG_n^o is the critical energy for a nucleus and k_B is Boltzmann's constant. The constants $I_{S,L}^o$ are related to nucleation kinetics.

The width of the diffuse interface can be envisioned as a balance between the opposing energy effects described by W and ε_φ. The former increases the energy of material on the boundary, which tends to make the interface sharp. The later increases the energy of rapidly changing φ which tends to make the interface more diffuse. Hence, these two parameters provide a means to shape the interface region for different problems and materials, e.g., the Λ-transition region or the interface region between the solid and liquid material during fuel melting.

The phase field model does not explicitly define the position of the interface, but rather includes it indirectly. This technique allows for complex interface shapes, volumetric heating and undercooling/superheating effects that can pose difficulties in other simulation techniques.

3. Results

3.1 Manara experiment

The current model is being compared with experiments done by D. Manara at the Institute for Transuranium Elements in Karlsruhe, Germany in which he obtains measurements of the melting transition in non-stoichiometric UO_2 [9]. The results of these experiments are published and compared with a computer model developed at the ITU [10]. These papers are used to guide and verify the development of the modelling technique in this work.

In the Manara experiment, a prepared sample of UO_2 is held in a high pressure buffer gas to suppress the possible effects of UO_3 evaporation. The sample is heated on one side with a combination of two lasers whose beams are homogenized by random mixing over a long fiber optic cable. One laser is used at lower power to slow and condition the cooling rate to prevent undercooling. This effect would complicate the modelling procedure. The other laser is used at higher intensity to heat the surface of the sample and induce melting. The surface temperature in the center of the pellet is then recorded using optical pyrometers.

The model described in Manara's work [11] is one dimensional in depth for a flat sample with heat transfer in the z direction. This simplified representation is taken as a starting point for the current model development.

3.2 Simulation

This model requires the solution of a set of highly non-linear differential equations. This was accomplished using commercial Finite Element Method [FEM] software, Comsol Multiphysics. In order to resolve the interface, the computational mesh spacing must be on the order of the interface thickness δ. The mesh must be very fine in the region of interest leading to a long computing time. Symmetries are therefore very useful to exploit.

The experimental setup measures the surface temperature at the centre of the pellet over the course of the experiment. This temperature is therefore the quantity of interest for verifying the model. In the present simulation, the sample is treated as axially symmetric. Furthermore, the radial effects are assumed to have little contribution to the behaviour along the axis of the pellet. The model therefore consists of a one-dimensional domain representing depth over which equations (2.1) and (2.2) are solved. The boundary conditions at the surface of the pellet is a heat flux from the laser minus radiative and conductive heat transfer into the buffer gas. The conductive heat transport is modeled simultaneously. The rear boundary is fixed at the initial condition, room temperature.

Material properties for this simulation were obtained from the Fink review [12]. In addition the interface width δ in (2.6) to (2.8) is taken to be 0.5μm, I_L^o and I_S^o in (2.9) is chosen to be 10 and 1, respectively; however, due to the exponential term, the model is not sensitive to these latter values. The functions ΔG_{fusion} and ΔH_{fusion} are taken from the FACT database.

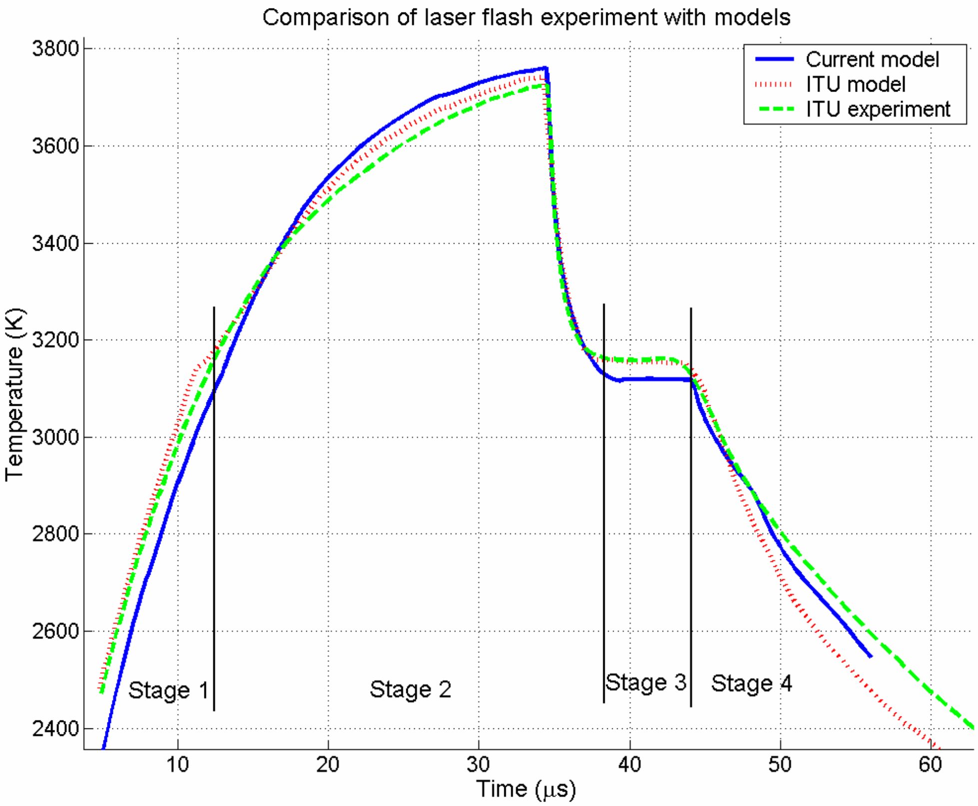

Figure 1:Surface temperature vs. time as divided into four stages. The difference in temperature plateaus is due to the a choice of the melting point at 3120 K (3147 K was recommended as a result of these experiments).

Figure 1 shows the results of the simulation compared to the measured values. Table 1show the calculated sequential depth profiles of the 1-D simulation. For interpretation purposes, the thermogram may be divided into four stages:

1. The sample is completely solid and being heated rapidly by the combined lasers pulse.

2. The surface temperature has passed the melting temperature. There are now two phases present; a liquid phase near the surface of the sample, and the bulk solid phase. The liquid phase grows with time until a maximum temperature is reached. After this point the heating laser is turned off and the sample cools rapidly until the free surface temperature reaches the melting temperature again. Concurrently, the liquid region is resolidifying against the underlying solid.

3. The free surface liquid temperature meets the melting temperature and starts to solidify. Solidification now advances from both the surface and the bulk into the liquid. The conditioning laser is used to prevent undercooling of the sample. As the liquid solidifies, the latent heat is released, which, combined with the conditioning laser, helps to keep the temperature at the surface approximately constant. This produces the observed plateau in temperature until all of the liquid is resolidified.

4. The liquid phase is now completely solidified and there is only the solid phase remaining. The temperature slowly becomes uniform over the sample. There is a kink in the temperature profile when the conditioning laser is turned off.

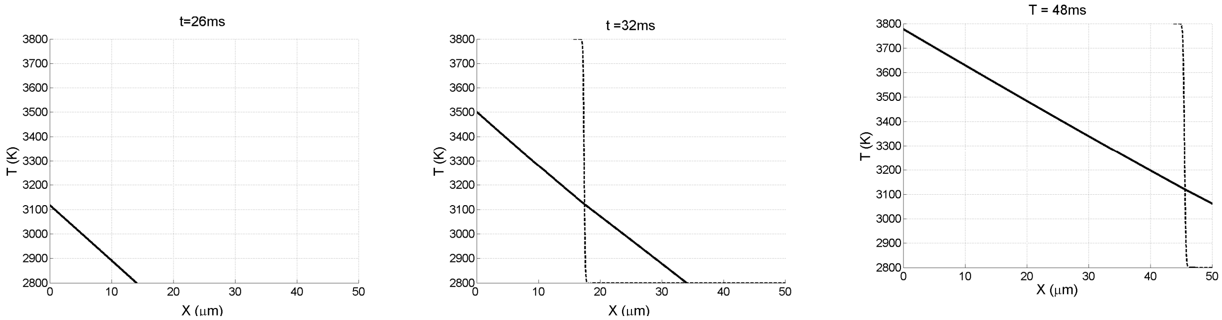

No molten region **Liquid phase has been created** **Liquid region is at maximum depth**

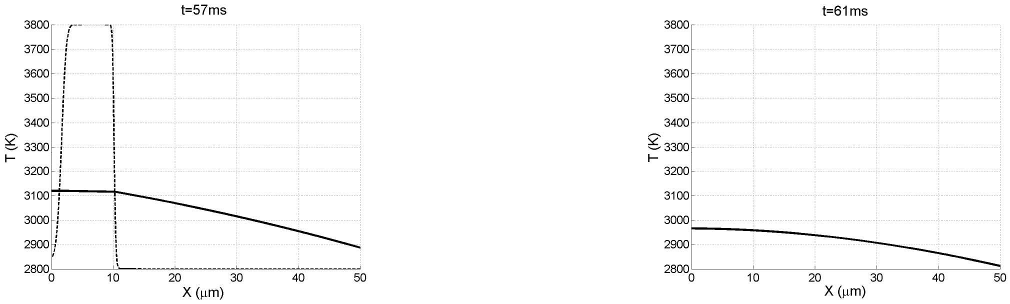

Liquid pool trapped between 2 solid regions **Entire sample solidified**

Table 1: Sequential progression of molten pool depth. Dotted line indicates φ ranging from 0 (solid) to 1 (liquid)

4. Conclusions and future work

The current results demonstrate that the suggested mathematical concept and implementation is sound. Material properties may be adjusted within the experimental uncertainty to better fit the data. This work has direct application to describing the centerline melting phenomenon in operating defective fuel elements with the presence of hyperstoichiometric (i.e., oxidized) fuel. In particular, the theory outlined here will be expanded to incorporate the effects of a solution of UO_2 and oxygen for hyperstoichiometric UO_{2+x}. These effects include non-congruent phase change and the Soret and Dufour effect. Future work will incorporate these effects in order to simulate non-congruent melting. The placement and thermal effects of the Λ-transition is being researched in parallel with this model development.

5. Acknowledgements

This work was funded by a Defence Research and Development Board [DRDB] scholarship and a Collaborative Research and Development grant from the Natural Sciences and Engineering Research Council of Canada [NSERC] and is being performed at The Royal Military College of Canada. I would like to thank my supervisors Dr. Lewis and Dr. Thompson for their guidance, advice and support. Also, I wish to thank Dr. Manara for his advice, discussions and data provided to me from his experiments at ITU.

A Phase field derivation

A.1 Derivation of the general equation

To determine the total entropy in a volume V, a general entropy functional is proposed in the form [13], [14]

$$S = \int_V \left(s(u,\varphi) - \frac{\varepsilon_\varphi^2}{2} \left| \vec{\nabla} \varphi \right|^2 \right) \mathrm{dV} \tag{A.1}$$

where $s(u,\varphi)$ is the local entropy density given as a function of the internal energy u and the phase field variable φ. The constant ε_φ characterizes the energy effect of a gradient in φ. Using dot notation to indicate time derivatives, the rate of change of the entropy functional may be derived.

$$\frac{\mathrm{d}S}{\mathrm{d}t} = \int_V \left(\frac{\partial s}{\partial u} \dot{u} + \frac{\partial s}{\partial \varphi} \dot{\varphi} - \varepsilon_\varphi^2 \vec{\nabla} \varphi \vec{\nabla} \dot{\varphi} \right) \mathrm{d}V \tag{A.2}$$

The first law of thermodynamics is applied via

$$\dot{u} + \vec{\nabla} \cdot \vec{j}_u = 0 \tag{A.3}$$

where $\vec{j}_u$ is the heat flux. This equation can be substituted into equation (A.2) and rearranged through Green's Theorem and the Divergence Theorem to yield (A.4).

$$\underbrace{\frac{\mathrm{d}S}{\mathrm{d}t}}_{\textit{Entropy change}} = \underbrace{\int_V \left(\vec{\nabla} \frac{\partial s}{\partial u} \cdot \vec{j}_u + \left[\frac{\partial s}{\partial \varphi} + \varepsilon_\varphi^2 \vec{\nabla}^2 \varphi \right] \dot{\varphi} \right) \mathrm{dV}}_{\textit{Entropy produced by irreversible processes}} - \underbrace{\int_A \left(\frac{\partial s}{\partial u} \cdot \vec{j}_u + \varepsilon_\varphi^2 \dot{\varphi} \vec{\nabla} \varphi \right) \cdot \hat{n} \, \mathrm{d}\partial A}_{\textit{Entropy flux across boundary}} \tag{A.4}$$

where A is the boundary of V.

As the entropy produced in a system is always positive for a real system and since equation (A.4) is valid for an arbitrary volume:

$$\dot{S}_{produced} = \vec{\nabla}\frac{\partial s}{\partial u}\cdot\vec{j}_u + \left[\frac{\partial s}{\partial \varphi} + \varepsilon_\varphi^2\vec{\nabla}^2\varphi\right]\dot{\varphi} > 0 \tag{A.5}$$

This inequality may be ensured by assuming:

$$\vec{j}_u = M_u \cdot \vec{\nabla}\frac{\partial s}{\partial u} \tag{A.6}$$

$$\dot{\varphi} = M_\varphi\left(\frac{\partial s}{\partial \varphi} + \varepsilon_\varphi^2\vec{\nabla}^2\varphi\right) \tag{A.7}$$

where M_u and M_φ are always positive [15]. It is important to note that equation (A.6) is phenomenological and will be shown to reduce to the well-known Fourier heat flux. The constants M_u and M_φ are kinetic parameters and couple the driving forces to the resulting fluxes.

The solution of the phase field model requires solving equation (A.3) and (A.7) subject to the flux expression in (A.6). These two equations are coupled by the expression of the entropy density function $s(u,\varphi)$.

A.2 The state functions

The general energy and entropy density equations for a pure material may be written as:

$$u(T,\varphi) = [1 - p(\varphi)]u_S(T) + p(\varphi)u_L(T) + K_u(\varphi) \tag{A.8}$$

$$s(T,\varphi) = [1 - p(\varphi)]s_S(T) + p(\varphi)s_L(T) + K_s(\varphi) \tag{A.9}$$

where $p(\varphi)$ is an interpolation function of the phase parameter such that $p(\varphi = 0) = 0$ and $p(\varphi = 1) = 1$. The functions $K_u(\varphi)$ and $K_s(\varphi)$ describe the effects of a mixture of two phases in the form of surface energy and entropy of mixing for a solution of solid and liquid phases. Assuming that the number of separate phase regions (such as solid nuclei in a liquid phase) is not large, $K_s(\varphi) \cong 0$. The form of these equations is arbitrary, insofar as it does not change the sharp interface limit and will be discussed further below.

A.3 Thermodynamic driving forces

The internal energy flux given in equation (A.6) may now be expanded by noting the definition of thermodynamic temperature [16], leading to the recovery of the Fourier conductive heat flux:

$$\frac{\partial s}{\partial u} = \frac{1}{T} \tag{A.10}$$

$$\begin{aligned}\vec{j}_u &= M_u \cdot \vec{\nabla}\frac{1}{T} = -\frac{M_u}{T^2}\vec{\nabla}T \\ &= -k \cdot \vec{\nabla}T\end{aligned} \tag{A.11}$$

where the thermal conductivity has been introduced as $k = M_u / T^2$. The rate of change of internal energy is assumed to be approximately equal to the enthalpy due to the small thermal expansion of condensed phases. Using $'$ to denote differentiation with respect to φ:

$$\begin{aligned} \dot{h}(T,\varphi) &\cong \dot{u}(T,\varphi) \\ &= \rho Cp\dot{T} + \left[p'(\varphi)\Delta H_{Fusion} + K'_u(\varphi)\right]\cdot\dot{\varphi} \end{aligned} \tag{A.12}$$

The application of the phase field model therefore involves the solution of the following coupled differential equations:

$$\begin{aligned} \dot{u} &= -\vec{\nabla}\cdot\vec{j}_u \\ \rho Cp\dot{T} &= -\left[p'(\varphi)\Delta H_{Fusion} + K'_u(\varphi)\right]\cdot\dot{\varphi} + \vec{\nabla}\cdot k\vec{\nabla}T \end{aligned} \tag{A.13}$$

In expanding equation (A.7), the $\frac{\partial s(u,\varphi)}{\partial\varphi}$ term requires the notion of the total derivative [17] in order to make use of equation (A.8) and (A.9).

$$\begin{aligned} \frac{\partial s(u,\varphi)}{\partial\varphi} &= \frac{Ds(u,\varphi)}{D\varphi} - \frac{\partial s}{\partial u}\frac{\partial u(T,\varphi)}{\partial\varphi} \\ &= \frac{\partial s(T,\varphi)}{\partial\varphi} - \frac{1}{T}\frac{\partial u(T,\varphi)}{\partial\varphi} \\ &= p'(s_L - s_s) - \frac{1}{T}\left[p'\cdot(u_L - u_s) + K'_u\right] \\ &= -\frac{1}{T}\left[p'\cdot(f_L - f_s) - K'_u\right] \end{aligned} \tag{A.14}$$

Where $f=u-Ts$ is the Helmholtz energy. Assuming the approximate equality between internal energy and enthalpy again, $\Delta G_{fusion}(T) \cong f_L(T) - f_S(T)$ and equation (A.7) becomes:

$$\dot{\varphi} = -M_{\varphi}\left(\frac{1}{T}\left[p'(\varphi)\cdot\Delta G_{Fusion}(T) - K'_f(\varphi)\right] - \varepsilon_{\phi}^{2}\vec{\nabla}^{2}\varphi\right) \tag{A.15}$$

A.4 Nucleation

The onset of a solid phase within a liquid requires a critical number of molecules to surmount a potential barrier and assemble in a specific configuration as a result of random thermofluctuations [18]. Nucleation may be properly simulated in compliance with statistical mechanics by Langevin-noise terms [19]; however, due to the relatively large scale of this application, elementary nucleation theory is instead inserted *ad hoc* into (A.15).

The Gibbs energy ΔG_n associated with the formation of a spherical embryo of n atoms, in the solid configuration, is comprised of the bulk and boundary energies:

$$\Delta G_n = v\Delta g + A\sigma \tag{A.16}$$

where A is the area bounding a volume v, σ is the surface energy and Δg is the Gibbs energy change per unit volume [20]. The volumetric term is negative below the melting point and increases in magnitude monotonically whereas the surface energy is always positive. For a small embryo, the surface energy increase will outweigh the volumetric decrease, preventing the embryo's growth. As depicted in Figure 2, there is a maximum in ΔG_n at which point the addition of molecules will reduce the total energy of the cluster and the embryo will begin to grow.

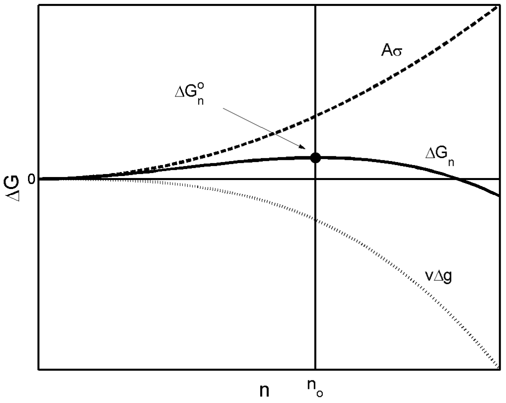

Figure 2: Embryo Gibbs energy as a function of n, showing the critical value

The maximum, ΔG_n^o for a spherical cluster is given as [21]:

$$\Delta G_n^o = \frac{16\pi}{3}\left(\frac{\sigma^3}{\Delta g^2}\right) f(\theta) \tag{A.17}$$

where *f(θ)* is the heterogeneous nucleation factor, a function of the wetting angle *θ*. This factor accounts for the reduction in nucleation activation energy by impurities, defects or foreign solids and greatly reduces the degree of undercooling during solidification.

Assuming an equilibrium concentration of nuclei and basic growth kinetics, an Arrhenius type expression for the nucleation rate may be derived:

$$I = I^o \exp\left(-\frac{\Delta G_n^o}{k_B T}\right) \tag{A.18}$$

where I_o is related to attachment kinetics and k_B is Boltzmann's constant.

The onset of liquid growth is assumed to behave in much the same way, except that the 'attachment' kinetics are much faster due to the restriction in solid molecules having to be attached to specific lattice sites.

Initial solid and liquid growth is incorporated into the phase field model by the addition of a source term into (A.15) which yields the expression for the time derivative of the phase change in equation (2.2):

$$\dot{\varphi} = -M_\phi\left(-\dot{\varphi}_n + \frac{1}{T}\left[p'(\varphi)\cdot \Delta G_{Fusion}(T) - K'_u(\varphi)\right] - \varepsilon_\varphi^2 \vec{\nabla}^2 \varphi\right) \tag{A.19}$$

$$\dot{\varphi}_n = \exp\left(-\frac{\Delta G_n^o}{k_B T}\right)\cdot \begin{cases} I_S^o(1-\varphi) & if\ \Delta G_{fus} < 0 \\ -I_L^o \varphi & if\ \Delta G_{fus} > 0 \end{cases} \tag{A.20}$$

A.5 Determining phase field constants

The choice of the interpolation function *p(φ)* and the excess interfacial energy $K_u(\varphi)$ are now investigated. Recall that *p(φ)* necessarily has properties that $p(\varphi = 0) = 0$ and $p(\varphi = 1) = 1$. The function K_u has the form of a double well potential having minima at $\varphi = 0{,}1$ and a maximum at

φ=0.5. The height of this potential barrier is proportional to a constant W which will be shown to relate to the surface energy later.

The Gibbs energy density may be derived from (A.8) and (A.9):

$$G(T,\varphi) = G_S(T) + p(\varphi)\cdot G_{fus}(T) + K_u(\varphi) \qquad \textbf{(A.21)}$$

We know that at the melting temperature G_S=G_L. Furthermore, in order to make the solid and liquid phase stable, $G(T,\varphi)$ must have local equilibriums at $\varphi = 0,1$ for all temperatures. Applied to equation (A.21) these constraints impart the following assertions on K_u and $p(\varphi)$ [22]:

$$\begin{gathered} K_u(0) = K_u(1) = 0 \\ \left[K_u'(\varphi) - p'(\varphi)\cdot G_{fus}\right]_{\varphi=0,1} = 0 \\ \left[K_u''(\varphi) - p''(\varphi)\cdot G_{fus}\right]_{\varphi=0,1} > 0 \end{gathered} \qquad \textbf{(A.22)}$$

Within the confines of these constraints, the actual form of these equations is arbitrary in that the choice does not affect the sharp interface limit. For this implementation, a common choice [8] is employed and plotted in Figure 3 and Figure 4.

$$p(\varphi) = \varphi^3[6\varphi^2 - 15\varphi + 10] \qquad \textbf{(A.23)}$$

$$K_u(\varphi) = W\varphi^2[1-\varphi]^2 \qquad \textbf{(A.24)}$$

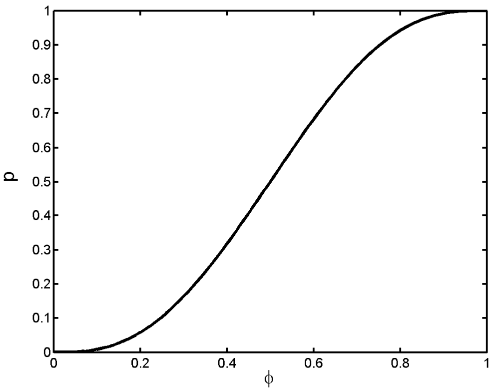

Figure 3: The interpolation function p(φ)

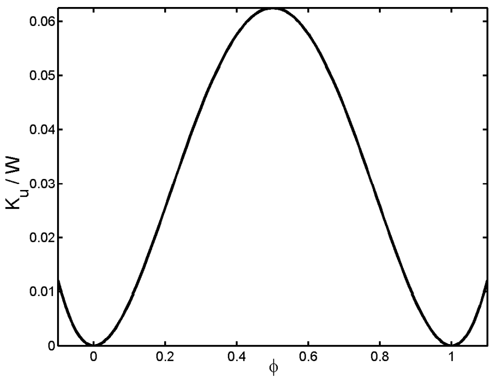

Figure 4: Double well potential function, K_u

It is now possible to use the sharp interface model to determine the constants W, ε_φ and M_φ and infer their meaning and physical relevance in doing so. To proceed, consider the case of an equilibrium solution in one dimension (planar interface) at the melting temperature T_m. The heat balance equation is satisfied and equation (A.19) becomes:

$$\begin{aligned} 0 &= -M_\phi\left(\frac{1}{T_m}\left[p'(\varphi)\cdot \Delta G_{Fusion}(T_m) - K_f'(\varphi)\right] - \varepsilon_\varphi^2\vec{\nabla}^2\varphi\right) \\ \varepsilon_\varphi^2\vec{\nabla}^2\varphi &= -\frac{2W}{T_m}\left[\varphi(\varphi-1)(2\varphi-1)\right] \end{aligned} \qquad \textbf{(A.25)}$$

for which a solution exists:

$$\varphi(x) = \frac{1}{2}\left[1 + \tan\left(\frac{x}{2\delta}\right)\right] \qquad \textbf{(A.26)}$$

where

$$\delta = \varepsilon_{\varphi}\sqrt{\frac{T_m}{2W}} \tag{A.27}$$

The constant δ can be interpreted as a measure of interface thickness as is shown graphically in Figure 5. This is a useful parameter to control since the mesh size for the computational domain must be of comparable size in order to adequately resolve the interface.

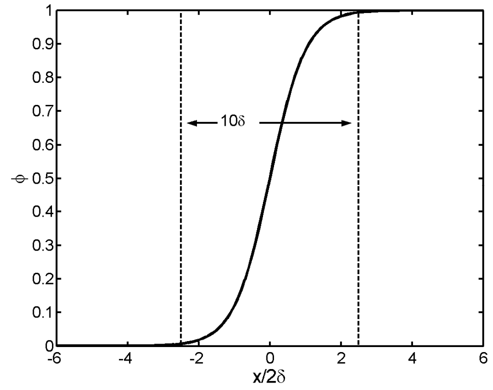

Figure 5: Steady state solution for φ

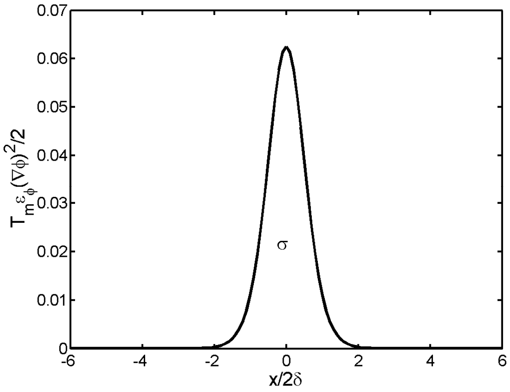

Figure 6: Excess energy

Assuming that the internal energy functional does not have any gradient components and using (A.1), the Gibbs energy functional may be written as:

$$G = \int_{\Omega}\left(g(T,\varphi) + T\frac{\varepsilon_{\varphi}^{2}}{2}\left|\vec{\nabla}\varphi\right|^{2}\right)\mathrm{d}\Omega \tag{A.28}$$

The excess energy term associated with the boundary, the surface energy, is given by the gradient term above. A plot of this energy over the steady state solution in (A.26) is shown in Figure 6. This can also be integrated to obtain an expression for the surface energy:

$$\sigma = \frac{\varepsilon_{\varphi}}{6}\sqrt{\frac{WT_m}{2}} \tag{A.29}$$

Equations (A.27) and (A.29) can be rearranged to determine expressions for W and ε_φ (i.e., as presented in equations (2.6) and (2.7) in Section 2):

$$W = 6\frac{\sigma}{\delta} \tag{A.30}$$

$$\varepsilon_{\varphi}{}^{2} = 12\frac{\sigma\delta}{T_m} \tag{A.31}$$

The mobility of the phase field, M_φ is related to the interface kinetics. The relationship between the accuracy of the solution and the interface width δ has been studied and an expression for M_φ that is accurate to second order in δ was derived. This expression is valid for equal liquid and solid conductivities and for small interface width.

$$\frac{1}{M_{\varphi}} = \frac{6\delta' H_{fus}}{T_m}\left[\frac{1}{\mu} + A\left(\frac{\delta H_{fus}}{k}\right)\right] \tag{A.32}$$

where μ is related to the surface attachment kinetics, $A \approx 5/6$, $\delta' = \delta / Tm$ and k is the thermal conductivity. Kinetic effects can be ignored by setting $\mu = \infty$, which makes (A.32) reduce to equation (2.8) as presented in Section 2: [8]

$$M_{\varphi} = \frac{k}{5}\left(\frac{T_m}{\delta H_{fus}}\right)^2 \qquad \textbf{(A.33)}$$

References

[1] Lewis B.J., Thompson W.T., Akbari F., Thompson D.M., Thurgood C., Higgs J., “Thermodynamic and kinetic modelling of fuel oxidation behaviour in operating defective fuel”, *J. Nucl. Mater.* 328 (2004) p180

[2] Hiernaut J.P., Hyland G.J., Ronchi C., “Premelting transition in Uranium Dioxide”, *International Journal of Thermophysics*, 14 (1993) 2 p259

[3] Cahn J.W., Hilliard J.E., “Free energy of a nonuniform system. I. Interfacial free energy”, *J. of Chem Phys*, 28 (1958) 2 p258.

[4] Hecht U., Gránásy L., Pusztai T., et al. “Multiphase solidification in multicomponent alloys”, *Materials Science and Engineering R* 46 (2004) p1-49.

[5] Welland M.J., Lewis B.L., Thompson, W.T. “Modelling the behaviour of UO_{2+x} during melting”, 30th CNS/CSA student conference, *CNS-SNC* (2006)

[6] Lupis C.H.P., “Chemical Thermodynamics of Materials”, *Elsevier Science Publishing Co., Inc.* New York, NY (1983).

[7] deGroot S.R. and Mazur P., “Non-equilibrium thermodynamics”, *General Publishing Company, Ltd.*, Toronto, ON (1984).

[8] Boettinger W.J., Warren J.A., Beckermann C., Karma A., “Phase-field simulation of solidification”, *Annu. Rev. Mater. Res.* 32 (2002) p163-194.

[9] Manara D., Ronchi C., Sheindlin M., “Pressure dependence of UO_2 melting measured by double-pulse laser heating”, *Journal of Nuclear Materials* 342 (2005) 148 p1147.

[10] Atrazhev V. and Brykin M., “Numerical simulation of melting and solidification of binary mixtures in laser heating pulses (non-congruent phase transition solid-liquid)”, Study Contract N. 17644-2001-03F1SC KAR RU Final Report (ITU).

[11] Manara D., “Melting transition measurements in Uranium Dioxide”, PhD thesis, University of Warwick, (2004).

[12] Fink J.K., “Thermophysical properties of uranium dioxide”,*Journal of Nuclear Materials* 279 (2000) p1.

[13] Penrose O., Fife P.C., “Thermodynamically consistent models of phase-field type for the kinetics of phase transitions”, *Physica D* 43 (1990) p44-62.

[14] Sekerka R.F., “Morphology: from sharp interface to phase field models”, *Journal of Crystal Growth*, 264 (2004) p530-540.

[15] Bi, Z., Sekerka R.F., “Phase-field model of solidification of a binary alloy”, *Physica A*, 261 (1998) p95-106.

[16] Huang F.F., “Engineering Thermodynamics: Fundamentals and Applications” *Macmillian Publishing Co, Inc.*, New York, NY (1976) .

[17] Arfken G and Weber H., “Mathematical methods for physicists”, Fifth Ed. *Academic Press* (2001).

[18] Cahn J.W., Hilliard J.E., “Free energy of a nonuniform system. III. Nucleation in a two-component incompressible fluid”, *J. of Chem Phys*, 31 (1959) 3 p688.

[19] Gránásy L., Pusztai T., Börzsönyi T., Tóth G., Tegze G., Warren J.A., Douglas J.F., “Phase field theory of crystal nucleation and polycrystalline growth: A review”, *J. Mater. Res.*, 21 (2006) 2 p309

[20] Herlach D.M. and Willnecker R., “Undercooling and solidification”, in book: “Rapidly solidified alloys”, ed: Liebermann, *Marcel Dekker Inc.*, New York, NY (1993)

[21] Fisher K., “Fundamentals of Solidification”, 4th Ed, *Trans Tech Publishing Ltd.* Uetikon-Zuerich, Switzerland (1998)

[22] Wang S.L., Sekerka R.F., Wheeler A.A., Murray B.T., Coriell S.R., Braun R.J., and McFadden G.B., “Thermodynamically-consistent phase field models for solidification”, *Physics D*, 69 (1993) p189-200